Reduction of water entry impact force by a gas jet

Yunhua Jiang[*]

School of Ocean Engineering and Technology, Sun Yat-sen University & Southern Marine Science and Engineering Guangdong Laboratory (Zhuhai), Zhuhai 519000, People's Republic of China and Key Laboratory of Comprehensive Observation of Polar Environment Sun Yat-sen University, Ministry of Education, Zhuhai 519082, People's Republic of China

Zhihui Zou

School of Ocean Engineering and Technology, Sun Yat-sen University & Southern Marine Science and Engineering Guangdong Laboratory (Zhuhai), Zhuhai 519000, People's Repubic of China

Lele Yang

School of Civil Engineering and Transportation, South China University of Technology, Guangzhou 510641, People's Republic of China

Le Shen

School of Naval Architecture, Ocean & Civil Engineering, Shanghai Jiao Tong University, Shanghai 200240, People's Republic of China

Yun Liu

Department of Mechanical and Civil Engineering, Purdue University Northwest, 1401 S. U.S. 421 Westville, Indiana 46391,USA

Mengqi Zhang[†]

Department of Mechanical Engineering, National University of Singapore, 9 Engineering Drive 1, 117575 Singapore

The violent hydrodynamic impact in water entry is a well-known phenomenon. Various methods have been applied to mitigate this "destructive force." We experimentally investigate a method for reducing the impact force of water entry, which uses a gas jet to impinge on the liquid surface prior to the object entry. The blowing of the gas jet flow forms a cavity in the water and the penetration of the object into the water is thus less impactful. This method also significantly alters the flow field structure in the impact region, resulting in a reduction of the added fluid mass, the counterthrust of the gas jet that can further attenuate the impact intensity. We reported four cavity regimes and six impact modes formed in the gas-liquid interaction for a range of the modified Froude numbers. In particular, the regime of jet cavity only has a jet-assisted water entry with almost no impact event, and the maximum reduction in impact acceleration can reach nearly 90% with the reduction in entry velocity being about 10% relative to the impact without gas jet. The impact force

---

[*]jiangyh35@mail.sysu.edu.cn
[†]mpezmq@nus.edu.sg

reduction mechanism is considered to be a combination of the reduction of the added fluid mass and the presence of gas jet momentum.

I. INTRODUCTION

Numerous studies on water entry exist in the fields of aviation and aerospace engineering, ocean engineering, and natural occurrences, such as seaplane and spacecraft water landings [1,2], hull slamming [3,4], as well as basilisk lizards running on the water surface, and stone skipping [5,6]. When the objects penetrate the water surface, a significant impact, accompanied by a complex change in the flow field, occurs at the initial stage of water entry. This impact can cause instrumentation, navigation trajectory, and even structural damage, especially in big-object high-speed water entry. In this investigation, we present and examine a method for reducing the impact force of water entry, as illustrated in Fig. 1, which utilizes a gas jet to impinge on the water surface prior to the sphere model entry [7]. In the following, we review the previous research on the water entry with some impact force reduction strategies and elucidate the application potential of our method in high-speed water entry.

The earliest experimental study of water entry was conducted by Worthington and Cole [8], who took instantaneous photographs to highlight the remarkable difference in the cavity flows of rough and smooth spheres entering the water. Previous literature concentrated on impact loads and primarily developed theoretical solutions for the nonlinear phenomenon. The impact load of the seaplane landing was calculated using the momentum theorem in Karman [1], who put forward the concept of the added or virtual mass in this problem. Subsequent works on the water entry impact load calculation included Bisplinghoff and Doherty [9], Cointe [10], and Zhao and Faltinsen [11]. Moreover, the specific flow modification caused by the penetrating object was recorded in some experiments. Specifically, the splash crown and cavity are the most salient flow structures in the water entry phenomenon. They are related to a remarkable effect of the impact force on the water surface [8,12,13]. In addition, from the perspective of fluid dynamics, the hydrodynamics of water entry is highly nonlinear and unsteady, in particular at the initial stage [14,15]. More specifically, the studies of sphere impact on the water surface indicate that the impact force grows rapidly to a maximum when penetration depth is $\sim$10–20% of the sphere radius and the impact drag coefficient is the function of the impact velocity [16,17]. Glasheen and McMahon [18] explained that the impact impulse is generated by the acceleration of the added fluid mass and showed that the drag force could increase by up to 76% at the later stage of water entry. Truscott et al. [19] investigated the unsteady force caused by a sphere entering the water and pointed out that the force is modulated by the cavity pressure in the cavity forming cases.

Prior research has demonstrated that nose geometry, impact velocity, entry angle, and material properties all play a role in reducing impact force [20–23]. More recently, some strategies for reducing the water entry impact load have been developed and tested by numerical calculations and experiments. For example, Vakarelski et al. [24] heated the sphere above the Leidenfrost temperature of a liquid and released it to water entry, and found that the drag force can be reduced by up to 85%. Elhimer et al. [25] showed that aeration considerably reduces the impact load. Speirs et al. [26] used a liquid jet before the sphere enters the water to reduce the relative velocity of the sphere to the quiescent liquid surface for impact force reduction. The experiment by Rabbi et al. [27] examined the impact force reduction by allowing two spheres to consecutively enter the water. Their results showed that the impact force for the second sphere can be reduced by up to 78%. However, previous works [26,27] focused on reducing the impact force of the initial stage of water entry, which may result in a secondary impact caused by the liquid jet being submerged or the cavity surface seal and deep seal due to the hydrostatic pressure [27,28].

Here, we experimentally investigate and check a different method for reducing the impact force utilizing a gas jet, which can reduce the impact throughout the whole water entry process. We examine the reduction of impact force and explain the reduction mechanism by inertial measurement unit (IMU), high-speed image, and particle image velocimetry (PIV). Compared with the model impact on the free water surface without gas jet, to be illustrated in Figs. 1(b) and 1(c), the gas jet continuously accelerates the water to form a cavity and alters the flow structure to prevent the sphere model from contacting the water directly. As long as the gas is supplied continuously, the gas from the nozzle can enclose the entire body under a specific gas ventilation volume. This proposed method can reduce not only the impact force, but also the friction drag at the later stage of water entry [29]. The paper is organized as follows. Section II describes the experimental details. In Sec. III, we report the experimental observation and explain the water entry cavity generated using a gas jet under different ventilation rates and entry velocities. Finally, the conclusion of the experimental results is provided in Sec. IV.

II. EXPERIMENTAL DETAILS

Our experiments were conducted in a water tank ($L \times W \times H = 1.8 \times 0.8 \times 1$ m) using a sphere model with a nozzle [as shown in Fig. 1(a)]. The nozzle is connected to a gas reservoir, with which a persistent gas jet can be provided during water entry. A schematic of the experimental setup is presented in Fig. 1. As the figure indicates, the sphere model connected by the gas tube falls freely using an electromagnet release mechanism. To help the sphere model fall vertically and minimize its rotation, two 0.8 mm steel wire ropes, positioned vertically, pass through the sphere model to guide its free-fall motion. The release mechanism is placed on an adjustable support to alter the free-falling height of the sphere model, so that the water entry velocity can be changed. The sphere model with a diameter D_s is attached to a cylinder to install an IMU, and the ventilation hole is connected to the nozzle with a diameter D_n. The whole model with a mass of M is made of aluminum.

The supply gas is generated by an air compressor, regulated by a gas flowmeter after passing through a buffer cylinder, and then the gas is transmitted to the sphere model through the gas tube for ejection. The air compressor can produce an air pressure of up to 8 Mpa at a flow rate of 240 L/min. The Omega FL2044 flowmeter, with a full scale of 100 SLPM and uncertainty of 3% at full scale, is used to measure the gas flow rate. The impact event is captured by the Photron FASTCAM Mini high-speed camera at 5000 fps, and the acceleration is recorded by the IMU nestled in the three-dimensional (3D) printed shell and fixed on the tail of the sphere model with a ventilation hole. For more accurate capturing of the impact peaks, the IMU uses a low-range three-axis accelerometer to record the impact acceleration at a sampling frequency of 2000 Hz, which is an MPU-6500 motion tracking device manufactured by InvenSense Inc. and is set to a maximum range of ± 16 g. Owing to the force from the gas tube and the steel wire ropes, the sphere model experiences small rotations during the free fall. Therefore, the impact acceleration magnitude of the total acceleration vector can be computed from measurements in the three axes.

The current problem concerns the interaction of a gas and free water surface, which forms a gas cavity during water entry by blowing a round gas jet from the end of the object. The Reynolds number, the nominal Weber number, and the blowing number are defined as $\mathrm{Re} = \rho_g U_{j0} D_n / \mu$, $\mathrm{We}_\eta = \rho_g U_{j0}^2 / \sqrt{\rho_l g \gamma}$, and $N_B = \eta^2 \mathrm{We}_\eta / 2$, respectively, where ρ_g is the density of the gas jet, U_{j0} is the mean velocity of the gas jet at the nozzle exit, μ is the air dynamic viscosity, ρ_l is the water density, g is the gravitational acceleration, γ is the surface tension of water, and, finally, $\eta = 0.447$ represents the ratio of the critical tangential velocity to the axial jet velocity [30]. In the scope of our experiments, we have $\mathrm{Re} \in [4.84 \times 10^3, 3.87 \times 10^4] > 2300$ and $\mathrm{We}_\eta \in [26, 1633]$. The Re is consistent with most of the reported data corresponding to turbulent jets. More importantly, large values of Reynolds number and nominal Weber number imply the surface instability behavior of splashing, oscillation, and swirling. Since the blowing number $N_B \in [2.6, 163.1]$ in this work, the gravity and inertia effects are dominant factors and the viscous and surface tension can be neglected
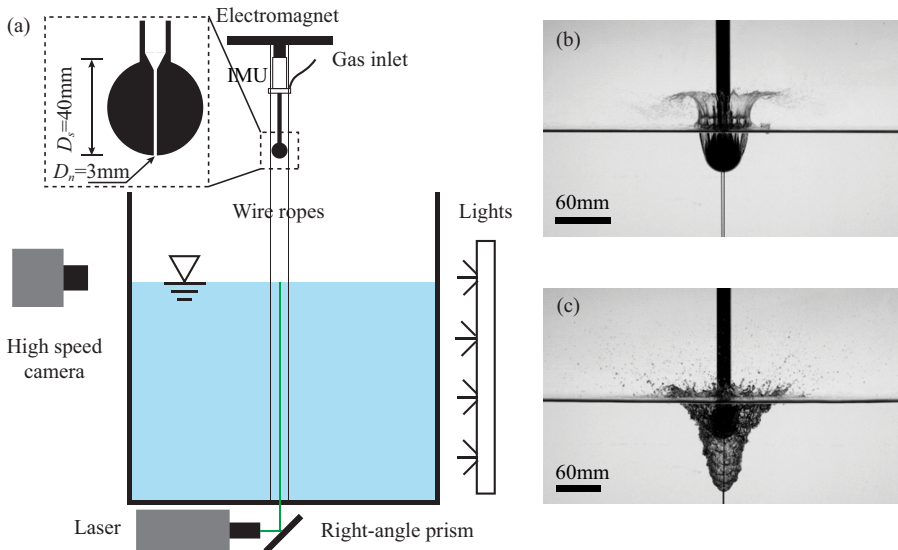
FIG. 1. (a) Schematic diagram of the experimental setup. (b) The sphere model impacts the free water surface without a gas jet at a velocity of $U_0 \approx 5.55$ m/s and forms a typical splash crown. (c) Water entry with a gas jet causes considerable agitation and then forms a rough cavity prior to the sphere model head, which encloses the sphere model under the condition of $U_{j0} \approx 141.47$ m/s, $U_0 \approx 5.16$ m/s [same falling height as (b)]. A part of the gas jet propels the water forward and part of it flows away along the cavity wall causing droplet splashing at the water interface.

due to the Kelvin-Helmholtz (K-H) instability criterion requiring $N_B > 1$ for the onset of splashing. For the gas jet impinging the water surface, a modified jet Froude number has been defined to be $\mathrm{Fr}_j = \rho_g U_{j0}^2 / \rho_l g D_n$ as the kinetic energy over the potential energy to describe the ratio of the inertial force to the buoyancy force of the injected gas [30–32]. Since the physical phenomenon depends on the jet velocity and entry velocity, we have also defined a modified Froude number, $\mathrm{Fr}^* = \mathrm{Fr}_j / \mathrm{Fr}_s$, to correspond to the effects of the inertial forces and gravity, where $\mathrm{Fr}_s = U_0^2 / g D_s$ is the sphere model Froude number.

Based on previous work, a 3 mm nozzle can produce a jet cavity with a diameter several times the cavitator diameter at a specific Froude number and momentum ratio [7,33]. Thus, in this work, the ratio of the nozzle diameter to the sphere model diameter is set to be $D_n / D_s = 0.075$. The volume flow rate Q under standard conditions (i.e., a temperature of 273 K and a pressure of 1 bar) ranges from 10 to 80 SLPM (standard liter per minute), resulting in U_{j0} from 23.58 to 188.63 m/s for the 3 mm nozzle. The impact velocity U_0 varies from 2.54 to 5.55 m/s according to the experimental image measurement. The modified Froude number Fr^* ranges from 0.29 to 90.50 across all the different gas jet flow rates and entry velocities. It is worth mentioning that U_0 is measured when the sphere model reaches the free surface, although the gas jet creates a cavity that postpones the impact event compared to the quiescent case (no gas jet). The uncertainty of all statistical results in this work is estimated at 95% confidence interval and we employ the Taylor series method (TSM) to propagate uncertainty [34].

III. RESULTS AND DISCUSSIONS

A. Cavity formation and impact force reduction

To illustrate the impact force reduction and cavity formation with a gas jet, we present in Fig. 2 the typical water entry high-speed images, the impact acceleration, and the velocity history of the
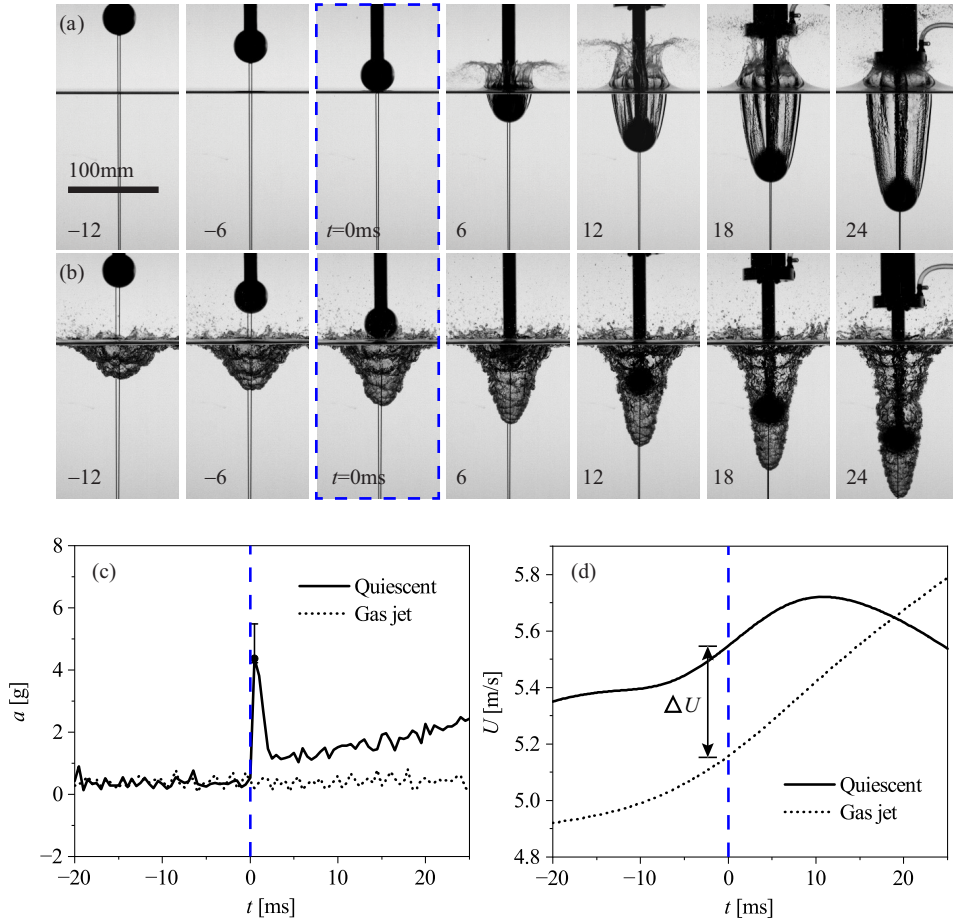
FIG. 2. (a) The sphere model impacts the free water surface at a velocity of $U_0 \approx 5.55$ m/s and experiences an open-cavity and surface seal phase. (b) The sphere model with a gas jet ($U_{j0} \approx 141.47$ m/s) penetrates the water surface with the entry velocity of $U_0 \approx 5.16$ m/s and forms a rough cavity named "jet cavity." (c) The measured acceleration a vs time t for the sphere model impacting a free surface without and with a gas jet, corresponding to (a) and (b), respectively. The blue dashed line indicates the time when the sphere model impacts the water surface in (a) or reaches the free surface in (b). (d) The velocity history of the sphere model corresponds to (a) and (b) during water entry. The $\Delta U \approx 0.38$ m/s is the velocity difference between these two cases. See the Supplemental Material, movies S1 and S2 [35]. These movies are recorded with 5 k fps and playback of 60 fps.

sphere model impact on the free water surface with and without the gas jet (more details can be found in the Supplemental Material, movies S1 and S2 [35]). As indicated in Figs. 2(a) and 2(c) for the case without a gas jet, the impact acceleration rises sharply to a maximum within 1 ms of approximately 4.37 g when the sphere model impacts on the water surface with a velocity of $U_0 \approx 5.55$ m/s. The impact process is accompanied by unsteady and violent hydrodynamic force [14,16]. After the impact, a splash curtain is formed with an opening cavity that elongates with the sphere model motion at an acceleration of approximately 1.5 g. Remarkably, the striated cavity walls are observed to be caused by the rough model surface as reported in Truscott *et al.* [15]. Moreover, owing to the size of the experimental setup, the model base meets the splash crown to form a secondary impact at approximately 20 ms (or see the instant at 24 ms in the figure).

Corresponding to the acceleration of the impact events as shown in Fig. 2(c), the acceleration of free falling is approximately 0 g. It should be emphasized that the surface seal and deep seal will occur for complete water entry [15,20], and the cavity ripples occasionally emerge after a deep seal [36]. Figure 2(b) shows an image sequence of a sphere model with a gas jet of $U_{j0} \approx$ 141.47 m/s impacting a free water surface at a velocity of $U_0 \approx 5.16$ m/s [the same releasing height as that in Fig. 2(a)]. The phenomenon of liquid droplet splash and the free surface oscillation are observed when the gas jet blows towards and reaches the free water surface, as shown in Fig. 2(b) at the moment before 0 ms. Note that the instant 0 ms corresponds to the lowest point of the sphere model touching the horizontal line of the water surface in this case. As the sphere model goes below the water surface, the gas jet continues to push the water to form a growing open cavity. It is worth noting that the interface of the formed cavity is rough and accompanied by fluctuations. We attribute this to the K-H instability when the gas jet interacts with the free surface to form a viscous shear layer as reported in Hwang and Irons [30] and Jiang *et al.* [7].

After the sphere model is completely immersed in the water, the whole sphere model is inside the cavity and the gas jet continues to push the surrounding liquid downward to develop a relatively stable cavity in front of the sphere model, as presented in Fig. 2(b) after 0 ms. Compared with the impact of that without a gas jet, there is almost no peak acceleration in the case of the impact with a gas jet, as shown in Fig. 2(c). Specifically, the sphere model impacting the water surface with a gas jet experiences an acceleration of approximately 0.43 g (including the friction drag from the steel wire) and reduces the impact force by about 90% compared to the quiescent impact. From these results, we can see that the gas jet is effective in reducing the water entry impact acceleration. Considering the impact acceleration might be reduced due to the counterthrust of the gas jet, it is necessary to compare the entry velocity of both cases (i.e., with and without a gas jet). More specifically, the corresponding entry velocity does not decrease much in the case of a gas jet where the velocity percentage reduction is only about 6.8% ($\Delta U / U_{\text{quiescent}}$) relative to the quiescent case corresponding to $\Delta U \approx 0.38$ m/s (at the instant of 0 ms), as shown in Fig. 2(d). Here, ΔU is the velocity difference of the sphere model reaching the water surface with and without a gas jet, and $U_{\text{quiescent}}$ is the U_0 without a gas jet. This result suggests that the impact acceleration can be significantly reduced by a gas jet while having a low velocity reduction. Furthermore, the gas jet follows the sphere model motion and keeps pushing the cavity forward, while the jet length diminishes for the water entry with a gas jet. Compared to the fixed gas jet that impinges on the water surface [37], the cavity depth deepens, the cavity seal occurs, and the jet length diminishes, caused by the sphere model motion and hydrostatic pressure for the water entry with a gas jet.

The moving velocity of the cavity pushed by the jet could be of interest. Quantitatively, the cavity moving velocity (U_c) can be obtained by considering the momentum balance between the jet and hydrostatic pressure at the impact point (the deepest of the cavity). Considering a kinematic model with the turbulent jet present in Fig. 3(a), the sphere model crosses the free surface located at z_1 and with a maximum depth of the cavity at z_2. The center-line velocity distribution of a free turbulent jet can be written as $U(z = z_2) = K U_{j0} D_n / (z_2 - z_1)$, where K is an empirical constant [37]. Clanet and Lasheras [38] have predicted the velocity at the distance $z_2 - z_1$ by applying conservation of the linear momentum, i.e., $U = U_{j0} D_n / [2(z_2 - z_1) \tan \alpha]$, where α is the opening angle of the jet. Note that U is considered to be a mean velocity in Clanet and Lasheras [38], whereas U in Banks and Chandrasekhara [37] refers to the velocity of a specific location at the center line. In particular, since both α and K are reported on a large scale, $K \approx 1/(2 \tan \alpha)$ holds. The momentum balance requires $\frac{1}{2} \rho_g U^2 (z = z_2) = \rho_l g z_2$, leading to the equation

$$z_2 (z_2 - z_1)^2 = \frac{K^2 \rho_g U_{j0}^2 D_n^2}{2 \rho_l g}. \tag{1}$$

So, one deduces the following approximate analytical solution:

$$\dot{z_2} = \dot{z_1} \left[1 - \frac{1}{2} \left(\frac{z_{20}}{z_{20} + z_1} \right)^{\frac{3}{2}} \right], \tag{2}$$
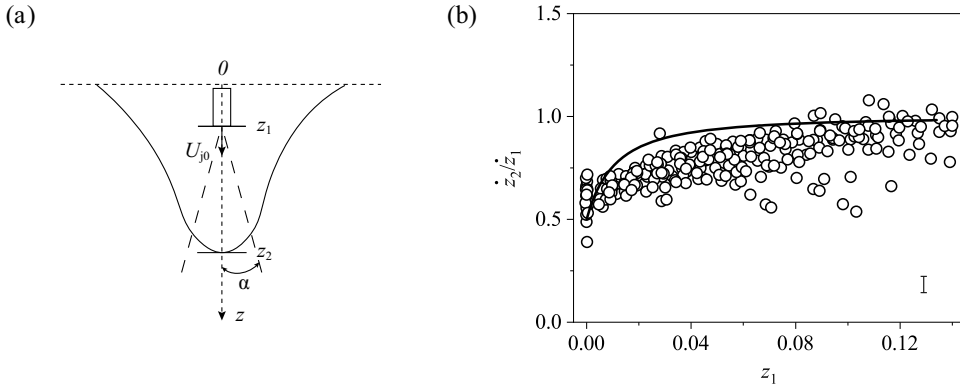
FIG. 3. (a) Schematic showing a turbulent jet penetrating the free surface. (b) The measured cavity moving velocity (U_c) evolution after the sphere model crosses the free water surface. The black solid line shows Eq. (2) at $\mathrm{Fr}_j \approx 835.6$. Characteristic error bars are shown.

where $z_{20} = [K^2 \rho_g U_{j0}^2 D_n^2 / (2 \rho_l g)]^{1/3}$. Since $U_c = \dot{z}_2$ and $U_{sphere} = \dot{z}_1$, Eq. (2) predicts that the velocity of the cavity is half the velocity of the source when $z_1 \ll z_{20}$ ($U_{sphere} \approx U_0$) and increases to the source velocity in the limit $z_1 \gg z_{20}$. Figure 3(b) depicts the theoretical prediction and experimental findings of U_c, demonstrating that the prediction can capture the moving cavity relatively well. It is noteworthy that z_{20} is proportional to $\mathrm{Fr}_j^{1/3}$, which indicates that the cavity velocity is not simply driven by the source velocity but also depends on the jet energy. In the case of a water jet entering the liquid pool [26,39], a cavity can be created by the water jet and the cavity velocity is approximately equal to half of the impact velocity, which is also the same as our experimental cavity moving velocity. Therefore, a reduction of the peak impact acceleration of the water entry with a gas jet may mainly be due to the relative impact velocity reduction between the sphere model and cavity as reported by Speirs *et al.* [26], which reduced by about 75% of the peak impact acceleration due to the relative impact velocity decrease caused by the water jet. It suggests that when the cavity velocity reaches the source velocity, the greatest force reduction is achieved.

B. Impact regimes and characteristics

We have shown above the impact acceleration reduction caused by the gas jet in the experiments. However, the reduction of impact acceleration is dominated by the relationship between the sphere model and the cavity geometry. Previous literature indicated that the depth and diameter of the cavity vary with the jet momentum at a specific spray distance [37,40]. In the current study, the nozzle follows the motion of the sphere model, which suggests the geometry of the cavity changes over time. Specifically, four different cavity regimes and six impact modes were observed in our experiments. The regimes are classified according to a combination of the impact velocity and the gas jet velocity, i.e., Fr^*. Following the definitions of Rabbi *et al.* [27] and Jiang *et al.* [7], the four cavity regimes are named shallow cavity [Fig. 4(a)], deep cavity [Fig. 4(b)], jet cavity [Fig. 4(c)], and closure cavity [Figs. 4(d)–4(f)], corresponding to six impact modes, i.e., on cavity [Fig. 4(a)], inside cavity [Fig. 4(b)], on jet [Fig. 4(c)], inside balloon [Fig. 4(d)], on balloon [Fig. 4(e)], and inside bowl [Fig. 4(f)]. Note that the regime of closure cavity includes three impact modes which are inside balloon, on balloon, and inside bowl, corresponding to the sphere model impact after, at, and before the pinch-off point, respectively. Both the schematics of these regimes and modes and their corresponding experimental results are provided in Fig. 4.

In detail, when the jet velocity is insufficient to yield the formed cavity opening diameter d_c (formed by the blowing jet at the free water surface when the sphere model reaches the free water surface) being smaller than the sphere diameter, the sphere model impacts the shallow cavity (i.e.,
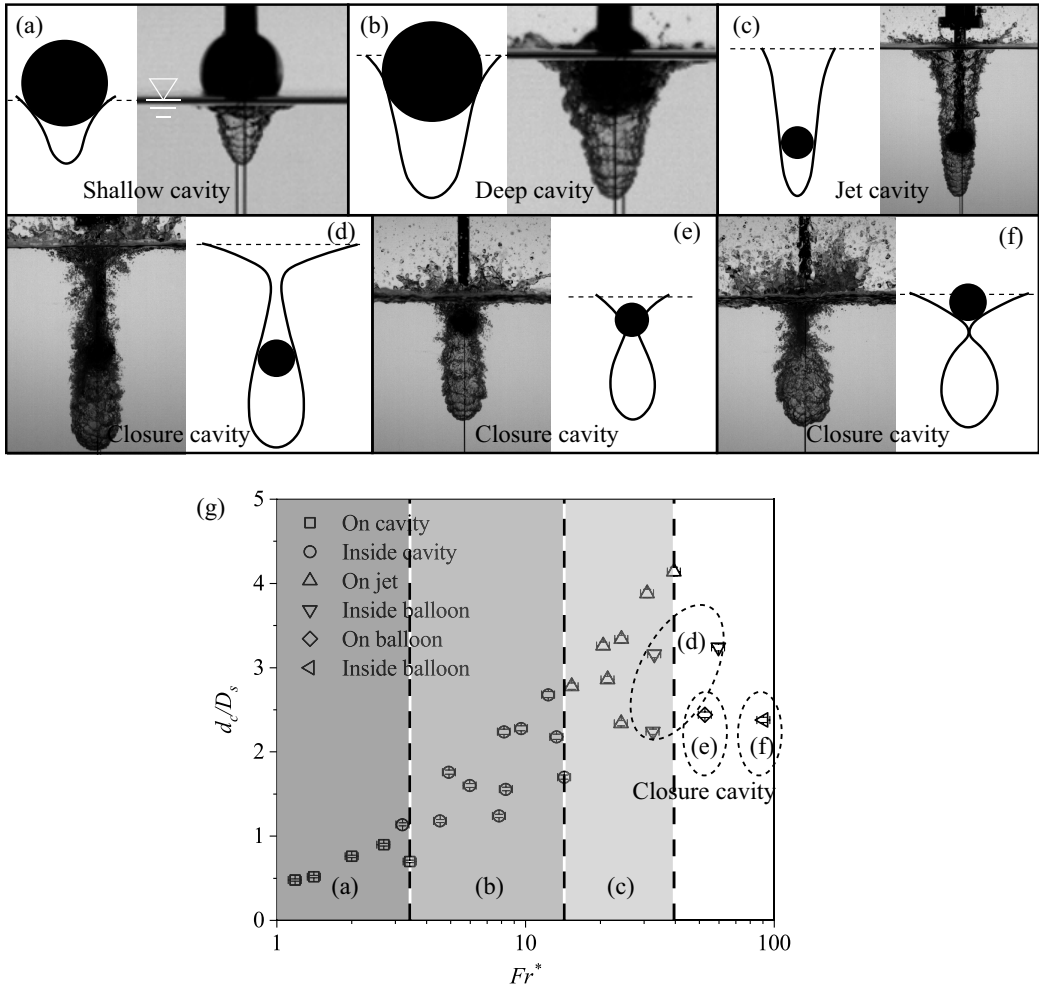
FIG. 4. Cavity and impact modes formed by gas jet classification under the different gas jet and water entry velocities. All schematics are shown with the corresponding experimental images. (a) Low jet velocity forms a shallow cavity and yields the impact mode called on cavity at $Fr^* \sim 2.7$. (b) Moderate jet velocity forms a deep cavity and the impact mode called inside cavity at $Fr^* \sim 6.0$. (c) A jet cavity formed without impact and the mode named on jet, $Fr^* \sim 21.4$. (d)–(f) The high jet velocity forms the closure cavity and the impact mode called inside balloon ($Fr^* \sim 32.5$), on balloon ($Fr^* \sim 52.6$), and inside bowl ($Fr^* \sim 90.5$), respectively. (g) The experimental regimes of the different cavity regimes and impact modes plotted by the open cavity diameter d_c/D_s vs modified Froude number Fr^*. The different color-filled areas denote the various cavity regimes and impact modes, delimited by the dashed vertical lines. The elliptical dashed circles represent cases belonging to the closure cavity for different impact modes, i.e., inside balloon, on balloon, and inside bowl.

on cavity for the impact model), as presented in Fig. 4(a). If the jet velocity is moderate but not enough to maintain a considerable cavity, the sphere model will touch the cavity wall (i.e., deep cavity for cavity geometry and inside cavity for the impact model), which makes the cavity collapse at the later stage, as presented in Fig. 4(b). Once a relatively stable cavity is generated, a jet cavity is formed and the sphere model falls downwards without impact (i.e., on jet for the impact model), as presented in Fig. 4(c). These three impact modes were also reported in Rabbi *et al.* [27] for two
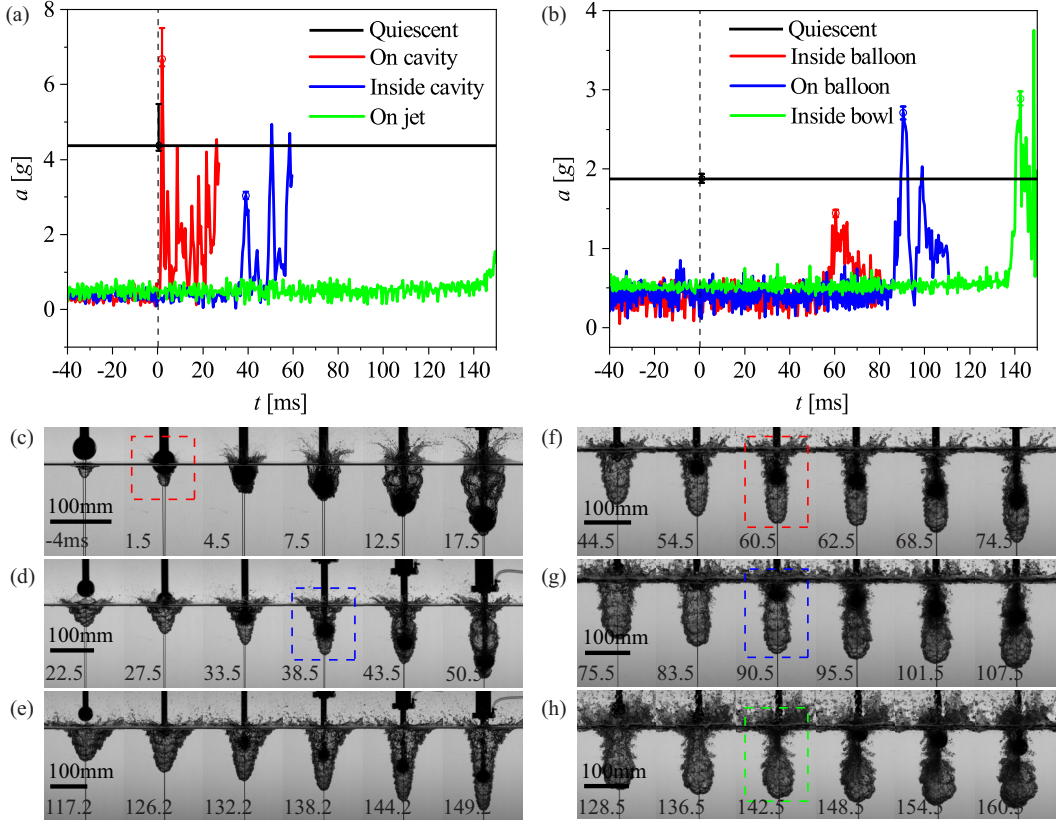
FIG. 5. The experimental measured acceleration and time series images for different impact modes with a gas jet. (a) The measurement acceleration for the cases of impact on the free water surface from a height of 1.8 m and (b) 0.6 m. (c)–(e) Corresponding experimental images of (a). (f)–(h) Corresponding experimental images of (b). The black solid lines denote the impact peak acceleration without a gas jet. The dashed lines in (a) and (b) denote the time that the sphere model reaches the water surface, and the dashed boxes in (c)–(e) and (f)–(h) indicate the impact state at the peak acceleration. The condition of these experimental images is $Fr^* \sim 2.7$, $Fr^* \sim 8.2$, $Fr^* \sim 20.5$, $Fr^* \sim 32.5$, $Fr^* \sim 52.6$, $Fr^* \sim 90.5$ for on cavity, inside cavity, on jet, inside balloon, on balloon, and inside bowl cases, respectively. The movies S3–S8 in the Supplemental Material are recorded with 5 k fps and playback of 60 fps [35].

consecutive falling spheres, in which the sphere interacts with a growing cavity (on cavity), the pre-pinch-off cavity (inside cavity), and the Worthington jet (on jet), respectively. The interaction mechanism in our case is consistent with theirs, the difference being that here the cavity is generated by the gas jet, which serves as an invisible "Worthington jet" exerting a reverse force on the sphere model, similar to the cavity generated by the first sphere water entry in Rabbi *et al.* [27]. It is worth pointing out that there is a distinct quick tendency for the cavity to go to a deep seal when the sphere model forms a seal cavity with the formed cavity. For the closure cavity, as shown in Figs. 4(d)–4(f), we observed three impact modes after, at, and before the pinch-off point, respectively. The cavity undergoes pinch-off as a result of the significant jet velocity matching the lower entry velocities, which results in the different impact modes of inside balloon, on balloon, and inside bowl.

From the observed closure behavior, this is different from the surface seal and deep seal created by general water entry. The surface seal is located near the water surface, while deep seal usually occurs at one-third to one-half cavity depth from the free surface [41]. The cavity closure event can also be named the shallow seal, which occurs relatively close to the free surface, and the pinch-off
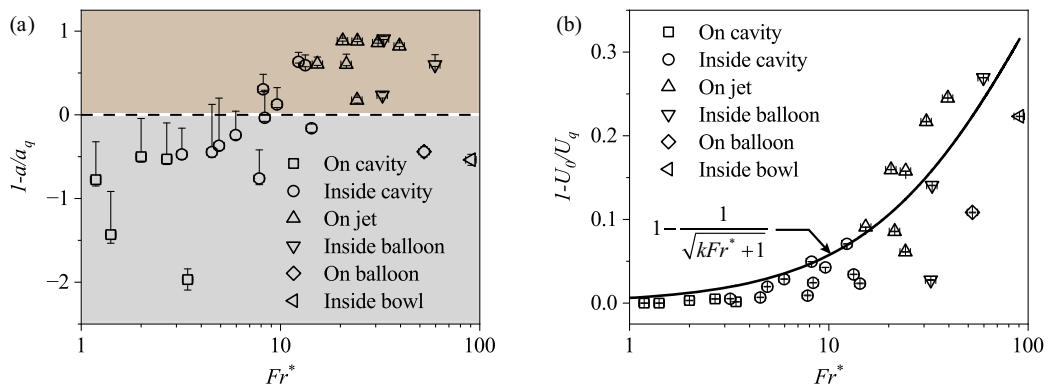
FIG. 6. The percentage reduction in (a) impact acceleration and (b) entry velocity at different drop heights. In the case of jet cavity, the impact acceleration percentage reduction can be up to $\approx 90\%$, while the velocity percentage reduction is only $\approx 10\%$. Here, a, U_0 are the peak acceleration and entry velocity (recorded when the sphere model reaches the free water surface) for gas jet cases, and a_q, U_q are the corresponding quiescent impact peak acceleration and entry velocity from the same drop height without a gas jet.

appearance is more like a deep seal [15,20]. The shallow seal in the work of Aristoff and Bush [20] is due to capillary instability, whereas the shallow seal is created by the jet, the same as the deep seal which is a hydrostatic pressure-driven collapse. Remarkably, the cases of closure cavity are similar to the consecutive sphere entry cases [27]. In their work, the first sphere opens the free surface to form a cavity, which experiences a deep closure, allowing the second sphere to interact with it. Similarly, the gas jet also works as an "object" to modify the liquid surface to create an opening cavity. There exist radial and axial expansion of the opening cavity formed by the sphere impacting the free water surface [20]. However, the air-entraining cavity formed by the gas jet mainly develops downward with the sphere model. Due to the velocity of a gas jet with Gaussian distribution [42], the radial growth of the cavity cannot be sustained by the jet-mixing layer which lacks momentum, shown in Fig. 8(a) (the velocity field distribution measured by the PIV). The cavity radial velocity growth of general impact is notably larger than the case of the gas jet impact. This implies that the
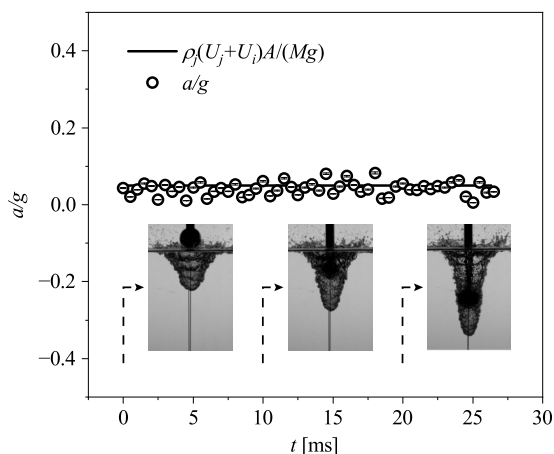

FIG. 7. The acceleration history of the sphere model for the case of jet cavity at $Fr^* \sim 12.3$. The solid black line indicates $\rho_j(U_j + U_i)^2 A/(Mg)$, where $\rho_j(U_j + U_i)^2 A$ is the gas jet thrust depicted by Eq. (5) and Mg is the weight of the sphere model. The black circles are the measured acceleration with error bar.
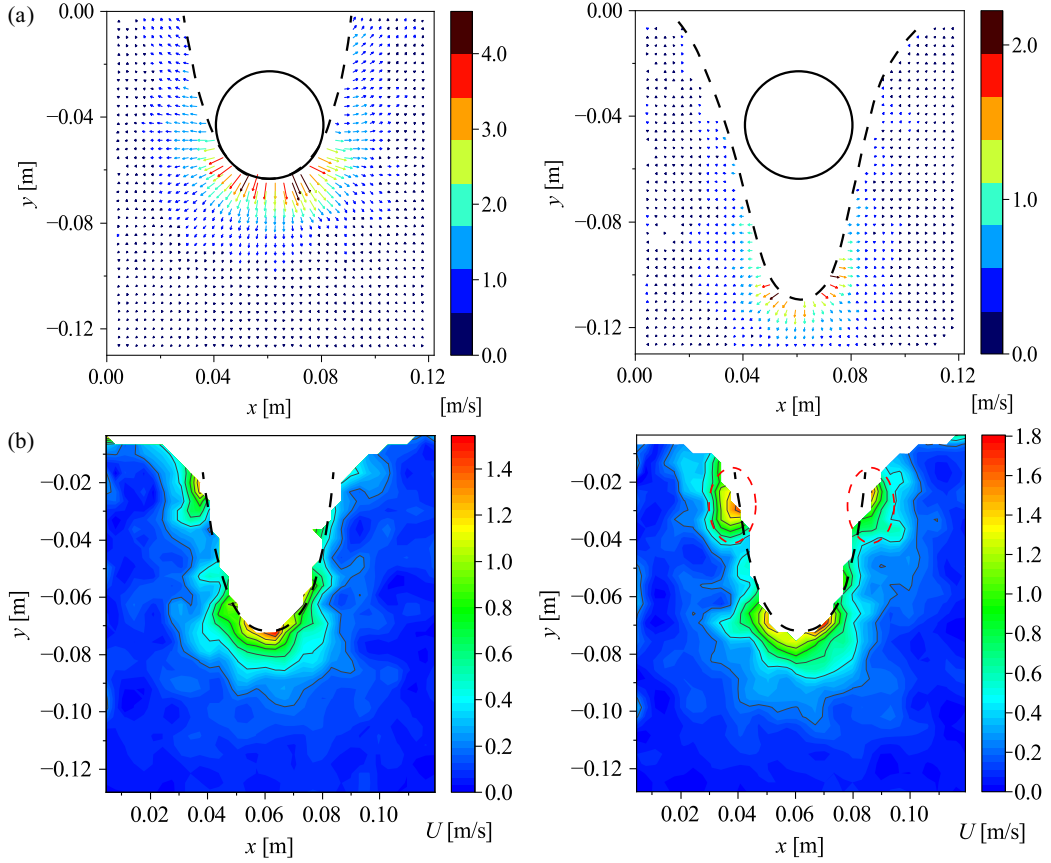
FIG. 8. (a) The impact region velocity vectors of the quiescent ($U_0 \approx 5.09$ m/s) and the gas jet impact ($U_0 \approx 4.87$ m/s, $U_{j0} \approx 117.9$ m/s) measured by PIV. (b) The velocity contour of the gas jet impact before and after the moment of the sphere model contact with the cavity wall under the entry velocity of $U_0 \approx 4.19$ m/s and $U_{j0} \approx 94.31$ m/s. The black dashed line is the outline of the formed air-entraining cavity. The red dashed circles indicate the impact regions.

air-entraining cavities produced by the gas jet as an "object" opening the free surface are more likely to deep seal than the cavity formed by the general case of the sphere impacting the liquid surface. In particular, at larger gas jet velocity, the high-speed jet rapidly pushes the liquid surface to the far front to form a larger cavity. The cavity without significant radial expansion quickly induces a surface seal forced by hydrostatic pressure [39,43], as indicated in Figs. 4(d)–4(f).

To further describe these cavity regimes and impact modes, we present the pattern transition in terms of the modified Froude number Fr* in Fig. 4(g). The vertical and horizontal coordinates denote the dimensionless cavity opening diameter d_c/D_s and Fr*, respectively. It is clear from the figure that the different cavity regimes and impact modes can be easily distinguished from the modified Froude number. At the low modified Froude number, it is difficult to form an open cavity with the gas jet, especially at high sphere model entry velocity. This is because the gas jet with small momentum dissipates severely with the higher incoming flow velocity (the direction of opposite model motion velocity). As the modified Froude number increases, the cavity opening diameter gradually increases and the cavity modes gradually change. In the case of the jet cavity of our interest, the modified Froude number is ~15.3–39.5 and the initial diameter of the formed open cavity is about ~2.5–4.0 times the sphere model diameter. In the jet cavity, although there is a gap between the sphere model

and the cavity wall, it is insufficient to allow a large amount of gas outflow along the cavity wall to resist the deep seal phenomenon at the rear of the sphere, as illustrated in Fig. 4(c). In addition, the cavity mode starts to change to a closure cavity when the modified Froude number is greater than the case of the jet cavity, and the reason for the smaller opening cavity diameter than those in all the other cases can be attributed to the premature deep seal.

For these impact modes, we discuss general impact scenarios and how we can obtain maximum acceleration reduction. Figures 5(a) and 5(b) present the impact acceleration over time under different impact modes (detailed information can be found in movies S3–S8 in the Supplemental Material [35]). The initial acceleration of the free falling is not zero due to the unfiltered data processing and the friction drag of the steel wire ropes. Figure 5(a) shows the acceleration of the different impact modes free falling at the same height of approximately 1.8 m. It can be seen that the initial impact pulse of the sphere model inside the cavity and on jet is less than the quiescent case (Figs. 5(a) and 5(c)–5(e); see the movies S3–S5 in the Supplemental Material [35]). In particular, the on jet case has almost no peak, indicating that a proper gas jet can greatly reduce the impact acceleration. Surprisingly, the acceleration peak of on cavity is significantly larger than that of the quiescent case. In addition to the counterthrust of the gas jet that may cause this result, the compression and expansion effect of the gas jet transient state may cause a larger impact peak, similar to the air cushion effects of Lin and Shieh [44], since the sphere model impacts the shallow cavity to form a closed region. The closure cavity regimes are likewise formed dropped at the same height of 0.6 m. Only in the case of inside balloon is the peak acceleration less than the quiescent case (Figs. 5(b) and 5(f)–5(h); see the movies S6–S8 in the Supplemental Material [35]), which impacts after the pinch-off point. In the cases of on balloon and inside bowl, as shown in Figs. 4(e) and 4(f), and Figs. 5(g) and 5(h) (see the movies S7 and S8 in the Supplemental Material [35]), the impact occurs at and before the pinch-off point, having a higher peak than the case of quiescent, which is attributed to the model impacting the fluid with significant upward momentum [27]. Since the impact occurs nearby the pinch-off point, the upward momentum in the on balloon case is less than that in the inside bowl case, yielding a peak acceleration that is slightly less. The peak acceleration of the inside balloon case is smaller than those in the other two cases due to only the sphere model tail experiencing the impact caused by the cavity pinch-off, as shown in Figs. 5(b) and 5(f) (see the movie S6 in the Supplemental Material [35]).

Now, we examine the percentage reduction of impact acceleration and entry velocities of the cases with a gas jet relative to the case without a gas jet. The acceleration and velocity percentage reduction are calculated as $1 - a/a_q$ and $1 - U_0/U_q$, respectively. Here, a and a_q are the measured peak acceleration for the case with and without a gas jet in the same experimental condition, respectively. U_0 is the velocity of the sphere model reaching the free water surface and U_q is the sphere model entry velocity without a gas jet. Figures 6(a) and 6(b) show the percentage reduction in acceleration and velocity across all the experimental different drop heights, respectively. As presented in Fig. 6, significant impact acceleration reductions are achieved in the inside cavity ($\sim 3.2 <$ Fr$^* < \sim 15.3$), on jet ($\sim 15.3 <$ Fr$^* < \sim 39.5$), and inside balloon ($\sim 32.5 <$ Fr$^* < \sim 59.6$) cases. In the case of jet cavity, the percentage reduction in acceleration can be up to $\approx 90\%$ at the modified Froude number of ~ 20.5, while the percentage reduction in velocity is only $\approx 10\%$, as illustrated in Fig. 6. To estimate the percentage reduction in velocity, the conservation of kinetic energy is evoked. More specifically, the gas jet has free jet properties before spreading to the water surface, and it is impeded only by shear stress with the surrounding fluid (i.e., the air above the water surface). The thrust contributed by the gas jet is $\dot{m}U_{j0}$ (kg m)/s^2, where $\dot{m}$ is the mass flow of the gas jet. Since the free gas jet forces the free water surface to deform, the force generated by the interaction between the gas jet and the water surface can be described as $k_0\dot{m}U_{j0}$ (where $0 \leqslant k_0 \leqslant 1$ is a variable that depends on the opening cavity shape) according to Mordasov and Savencov [45]. Thus, the conservation of kinetic energy can be written in a simplified way as $(F - k_0\dot{m}U_{j0})H = \frac{1}{2}MU_0^2$, where F is the total force due to the gravity and the friction drag of the steel wire, H denotes the height of the free-falling drop, and M is the mass of the sphere model. Then, a relationship exists between the modified Froude number and

the entry velocity, i.e., $1 - U_0/U_q = 1 - 1/\sqrt{k\mathrm{Fr}^* + 1}$ with $k > 0$. Figure 6(b) presents the fitting curve based on the experimental data resulting in $k \sim 1.25 \times 10^{-2}$, indicating that the maximum percentage reduction of the entry velocity only reaches $\approx 6\%$ to $\approx 25\%$ with $\approx 15\%$ to $\approx 90\%$ impact acceleration percentage reduction at the modified Froude number of ~ 15.3 to ~ 39.5.

C. Impact force increase and reduction mechanism

To explore the underlying physical mechanism of the impact peak acceleration reduction and increase across these impact modes (i.e., on cavity, inside cavity, on jet, inside balloon, on balloon, and inside bowl), the impact modes are categorized into three types for the subsequent analysis. The first group includes the on cavity and inside cavity cases, which are inertially dominated and the sphere model interacts with fluid during water impact. The second group represents the jet cavity and inside balloon cases, which are dominated by the jet force and fall almost under the action of the gas jet. The third group comprises the on balloon and inside bowl cases, which are governed by the inertia force and jet force, and the sphere model interacts with the impacted fluid with upward momentum [27].

Here we apply the momentum conservation theorem to a control volume consisting of the sphere model and the gas jet. In this control volume, the gas flow along the pipe inside the sphere model has a steady inflow and outflow, i.e., the outflow momentum is equal to the inflow momentum. Specifically, the mass of the injection gas is m_j in the control volume before the impact transient, and the amount of change in mass of the gas after the impact is δm_j. For the cases of on cavity and inside cavity, $MU_i + m_j(U_j + U_i) = (M + m)U + (m_j + \delta m_j)(U_j + U)$ can be used to describe the conservation of momentum during water impact, where M is the mass of the sphere model, U_i is the impact velocity, U_j is the outflow velocity of the gas jet, U is the instantaneous velocity of the sphere model after the impact, and m is the added fluid mass during impact. Following the deviation of Shiffman and Spencer [46], the vertical force of water entry with a gas jet for the on cavity and inside cavity cases (the m_j/M and $\delta m_j/M$ can be ignored assuming the body force of gas is sufficiently small; see the Appendix for the detailed derivation) is given as

$$F_z = \frac{(U_j + U_i) + \frac{m}{M}U_j}{\left(1 + \frac{m}{M}\right)^2} \frac{d\delta m_j}{dt} + \frac{1}{\left(1 + \frac{m}{M}\right)^3} \frac{U_i^2}{R} \frac{dm}{db}, \tag{3}$$

where R is the sphere model radius, $b = s/R$, and s is the submerged depth from the free surface. The first term on the right side ($d\delta m_j/dt$) is the mass flow rate of the gas jet during impact. The classical impact force of a sphere impacting the free water surface without a gas jet is given by Shiffman and Spencer [46],

$$F_z = \frac{1}{\left(1 + \frac{m}{M}\right)^3} \frac{U_i^2}{R} \frac{dm}{db}. \tag{4}$$

Comparing Eqs. (3) and (4), the impact force for the cases with a gas jet has an additional term of the gas jet thrust $(U_j + U_i)d\delta m_j/dt$ (assuming m/M is small and may be neglected) and first-order dependence on the rate of change of the added mass, dm/db. Thus, it is intuitive to understand that the impact force in the cases of on cavity and inside cavity is greater than that quiescent case because of the jet thrust [see Figs. 5(a) and 6(a)]. However, in some inside cavity cases, there is still a reduction in impact force, as shown in Fig. 6(a), at the modified Froude number of ~ 8.2 to ~ 15.3. For the impact with a cavity, the dm/db of on cavity and inside cavity is less than that of the quiescent case [27]. The contact surface of the sphere model with the cavity wall is different, resulting in different dm/db over a range of Froude numbers. With the impact force governed by both the jet thrust and dm/db, it means that the dm/db reduction may be greater than the amount of jet thrust to some extent, resulting in a reduction in impact force for some inside cavity cases.

To describe the conservation of momentum at any time, the added fluid mass term m should be excluded for the cases of the jet cavity and inside balloon without impact, i.e., $MU_i + m_j(U_j + $

$U_i) = MU + (m_j + \delta m_j)(U_j + U)$. Note that U_i should not be considered as impact velocity here, but the velocity at any instant when using the momentum conservation theorem. Applying the same derivation and simplification (see, again, the Appendix for a detailed derivation), we can obtain

$$F_z = (U_j + U_i)\frac{d\delta m_j}{dt}. \tag{5}$$

As indicated in Eq. (5), the vertical force equals the gas jet thrust. Therefore, it has no significant impact, creating a dramatic reduction with near zero peak acceleration for the cases of the jet cavity and inside balloon, as shown in Figs. 5 and 6(a). The peak acceleration of the inside balloon is less than that of the impact without a gas jet, but larger than the one of the jet cavity case, which can be attributed to the cavity seal interacting with the rear body of the sphere model in some inside balloon cases. Namely, the pinch-off of the air-entraining cavity divides the cavity into two parts: a growing air cavity maintained by the gas jet attached to the downwards moving sphere model and an upwards moving collapse cavity. Generally, the case of the inside balloon is effectively a closed jet cavity. Moreover, a more formal and accurate description in Eq. (5) would be $\dot{m}(U_j + U_i)$, where $\dot{m} = \rho_j(U_j + U_i)A$ (A is the cross-sectional area of the nozzle exit) is the mass flow of the gas. Equation (5) and the acceleration from experiments are presented in Fig. 7, which indicates that the jet thrust is the only source of vertical force other than gravity for the jet cavity case.

In addition, the momentum conservation theorem should consider the upwards momentum $M_{up} = mU_m$ for the cases of on balloon and inside bowl, as Rabbi *et al.* [27] reported, i.e., $MU_i + m_j(U_j + U_i) - mU_m = (M + m)U + (m_j + \delta m_j)(U_j + U)$, where U_m is the average velocity of the added fluid mass just before impact. Then a similar simplification (see the Appendix for the detailed derivation) for the vertical force can be written as

$$F_z = \frac{(U_j + U_i) + \frac{m}{M}(U_j - U_m)}{\left(1 + \frac{m}{M}\right)^2}\frac{d\delta m_j}{dt} + \frac{\left(1 + \frac{U_m}{U_i}\right)\left(1 - \frac{m}{M}\frac{U_m}{U_i}\right)}{\left(1 + \frac{m}{M}\right)^3}\frac{U_i^2}{R}\frac{dm}{db}. \tag{6}$$

This vertical force depends on U_m except for the jet thrust and the rate of change of the added fluid mass dm/db, as indicated in Eq. (6). The high-speed gas jet collides with the reverse momentum, and the value of dm/db is larger than that of the impact without gas jet, even though the gas jet has a slowing effect [47]. Therefore, the impact force in the on balloon and inside bowl cases is larger than that in the quiescent case due to the combination of the upward momentum and jet thrust.

To further understand the impact details of water entry with a gas jet, some PIV measurement results are presented in Fig. 8. The PIV configuration includes a 10 W and 532 nm green continuous wave (cw) laser with right-angle prisms located below the water tank which is seeded with silver-coated hollow glass spheres with a diameter of 5–20 μm, as illustrated in Fig. 1. The PIV analysis is performed using the open-source code developed by Thielicke and Sonntag [48] and the images were taken with the interframe spacing of 0.25 ms and processed with three passes at 64×64, 32×32, and 16×16 pixel interrogation regions, respectively. The added fluid mass depends on the mass of water entrained by the water entry sphere model [49]. The impact region velocity vectors of the water measured by the PIV under the quiescent impact without a gas jet ($U_0 \approx 5.09$ m/s) and the gas jet impact ($U_0 \approx 4.87$ m/s, $U_{j0} \approx 117.9$ m/s) are shown in Fig. 8(a). The gas jet impact on the water surface mainly pushes the water downward movement and the movement velocity of the water is significantly less than that of the sphere model directly impacting the free water surface. In addition, the cavity created by a gas jet provides less initial impact area and its downward movement velocity reduces the relative velocity between the sphere model and the water (i.e., $U_c \approx 0.5U_0$), which is similar to the water jet impact force reduction mechanism [26]. Practically, the added fluid mass effect caused by the gas jet does not change appreciably during the instantaneous impact, as shown in Fig. 8(b). This indicates that the morphology of the cavity generated by the gas jet is nearly identical before and after the impact. So, the cavity shape and velocity field can be used to clarify that the value of m is sufficiently small before and after the impact. For the specific case in Fig. 8(b), the velocity contour images are selected before and after the impact instant to present the fluid variation

around the jet under entry velocity $U_0 \approx 4.19$ m/s and gas jet velocity $U_{j0} \approx 94.31$ m/s. It can be seen that the velocity field difference between before and after the impact with a magnitude of only $\sim 10^{-2}$ and the cavity shape is almost unaltered at the moment of impact. For the hemispherical nose, Shiffman and Spencer [46] indicated that m/M compared to 1 can be neglected, not to mention that it now only interacts with the cavity wall.

IV. CONCLUSION

This paper reports a technique of using a gas jet to reduce the impact force of water entry, complementing similar methods in the literature by Rabbi *et al.* [27] and Speirs *et al.* [26]. Induced pressure and air-entraining cavities are formed when the insoluble gas impinges on the free water surface. The gas jet penetrating the free surface to form the opening cavity significantly changes the flow field structure of the impact regions reducing the added mass during water impact.

In this study, the gas jet has been shown to be effective in reducing impact force. Experimental results show that the gas jet forming different cavity regimes (i.e., shallow cavity, deep cavity, jet cavity, and closure cavity) over a range of specific modified Froude numbers produces different impact modes (i.e., on cavity, inside cavity, on jet, inside balloon, on balloon, and inside bowl). Specifically, a shallow cavity interacts with the sphere model to cause the impact mode of on cavity under a modified Froude number ($\sim 1.2 < \text{Fr}^* < \sim 3.2$). As the modified Froude number increases, the diameter of the opening cavity increases. Once the opening cavity diameter is larger than the diameter of the sphere model, the sphere model interacts with the cavity walls, leading to the inside cavity case ($\sim 3.2 < \text{Fr}^* < \sim 14.3$). The jet cavity is created with a further increase of modified Froude number ($\sim 14.3 < \text{Fr}^* < \sim 39.5$), which has almost no impact except the reverse thrust of the gas jet. The closure cavity is formed when the modified Froude number increases to some extent ($\sim 32.5 < \text{Fr}^* < \sim 90.5$), corresponding to the water impact that occurs before (inside bowl), at (on balloon), and after (inside balloon) the pinch-off point. The jet cavity formed at a modified Froude number of about 20.5 is of interest which is almost no peak acceleration, with a maximum percentage reduction in the acceleration of up to about 90% and a percentage reduction in entry velocity of only about 10% relative to the quiescent impact case. In addition, the reasons for the reduction of impact force are analyzed and explained in terms of the different impact modes. In the on cavity and inside cavity cases, the gas jet is responsible for slowing down the water entry velocity, while the formation of the opening cavity is responsible for the reduction of the added fluid mass of the water impact. The gas jet thrust in the jet cavity and inside balloon cases dominates the impact force. In the on balloon and inside bowl cases, the impact force is contributed to the ratio of jet velocity to entry velocity, added fluid mass, and upward fluid momentum simultaneously due to the upward fluid momentum created by the cavity closure behavior.

ACKNOWLEDGMENTS

APPENDIX: DERIVATION OF THE VERTICAL FORCE OF WATER ENTRY WITH GAS JET

To facilitate an in-depth understanding of the vertical force of water entry impact, this Appendix gives a detailed derivation by using the momentum theorem as follows and a schematic diagram is presented in Fig. 9(a). By categorical analysis, we have three equations for the conserva-
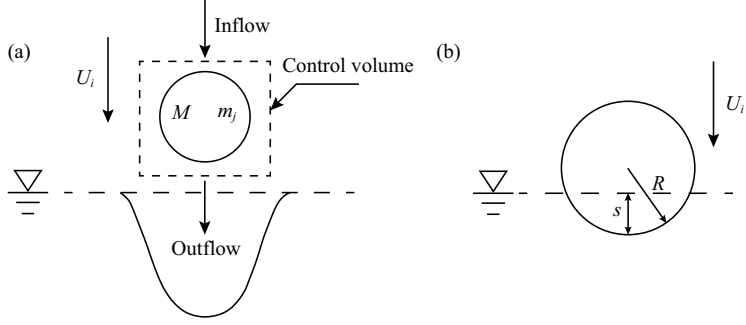
FIG. 9. (a) Schematic diagram of a sphere model water entry with a gas jet using the momentum theorem and (b) sphere penetrating the water surface.

tion of momentum, i.e.,

$$MU_i + m_j(U_j + U_i) = (M + m)U + (m_j + \delta m_j)(U_j + U) \tag{A1}$$

for the cases of on cavity and inside cavity,

$$MU_i + m_j(U_j + U_i) = MU + (m_j + \delta m_j)(U_j + U) \tag{A2}$$

for the jet cavity and inside balloon cases, and

$$MU_i + m_j(U_j + U_i) - mU_m = (M + m)U + (m_j + \delta m_j)(U_j + U) \tag{A3}$$

for the cases of on balloon and inside bowl. The vertical force during water entry is given by

$$F_z = -M\frac{dU}{dt}, \tag{A4}$$

solving Eq. (A1) for U and, taking the derivative concerning time, the $[\frac{dU}{dt}]_1$ can be given as

$$\left[\frac{dU}{dt}\right]_1 = -\left[\frac{(M + m_j)(U_j + U_i) + mU_j}{(M + m + m_j + \delta m_j)^2}\frac{d\delta m_j}{dt} + \frac{(M + m_j)U_i - \delta m_j U_j}{(M + m + m_j + \delta m_j)^2}\frac{dm}{dt}\right]. \tag{A5}$$

Combining Eqs. (A4) and (A5), the force during water entry is given by

$$[F_z]_1 = \frac{\left(1 + \frac{m_j}{M}\right)(U_j + U_i) + \frac{m}{M}U_j}{\left(1 + \frac{m + m_j + \delta m_j}{M}\right)^2}\frac{d\delta m_j}{dt} + \frac{\left(1 + \frac{m_j}{M} - \frac{\delta m_j}{M}\frac{U_j}{U_i}\right)^2}{\left(1 + \frac{m + m_j + \delta m_j}{M}\right)^3}\frac{U_i^2}{R}\frac{dm}{db}, \tag{A6}$$

where R is the sphere model radius, $b = s/R$, and s is the submerged depth from the water free surface [46], as illustrated in the Fig. 9(b). The derivatives are related by

$$\frac{d()}{dt} = \frac{d()}{db}\frac{db}{ds}\frac{ds}{dt} = \frac{U}{R}\frac{d()}{db}. \tag{A7}$$

Applying the same derivation to Eqs. (A2) and (A3), we have

$$\left[\frac{dU}{dt}\right]_2 = -\frac{(M + m_j)(U_j + U_i)}{(M + m_j + \delta m_j)^2}\frac{d\delta m_j}{dt}, \tag{A8}$$

$$\left[\frac{dU}{dt}\right]_3 = -\left[\frac{(M + m_j)(U_j + U_i) + m(U_j - U_m)}{(M + m + m_j + \delta m_j)^2}\frac{d\delta m_j}{dt}\right.$$
$$\left. + \frac{(M + m_j)(U_i + U_m) - \delta m_j(U_j - U_m)}{(M + m + m_j + \delta m_j)^2}\frac{dm}{dt}\right]. \tag{A9}$$

So, the vertical force can be given by

$$[F_z]_2 = \frac{\left(1 + \frac{m_j}{M}\right)(U_j + U_i)}{\left(1 + \frac{m_j + \delta m_j}{M}\right)^2}\frac{d\delta m_j}{dt},$$ (A10)

$$[F_z]_3 = \frac{\left(1 + \frac{m_j}{M}\right)(U_j + U_i) + \frac{m}{M}(U_j - U_m)}{(1 + \frac{m + m_j + \delta m_j}{M})^2}\frac{d\delta m_j}{dt}$$

$$+ \frac{\left[1 + \frac{m_j}{M} - \frac{\delta m_j}{M}\frac{U_j}{U_i} + \left(1 + \frac{m_j + \delta m_j}{M}\right)\frac{U_m}{U_i}\right]\left(1 + \frac{m_j}{M} - \frac{\delta m_j}{M}\frac{U_j}{U_i} - \frac{m}{M}\frac{U_m}{U_i}\right)}{\left(1 + \frac{m + m_j + \delta m_j}{M}\right)^3}\frac{U_i^2}{R}\frac{dm}{db}.$$ (A11)

Ignoring the terms m_j/M and $\delta m_j/M$ as a result of the sufficiently small body force of gas, Eqs. (A6), (A10), and (A11) can be rewritten as

$$[F_z]_1 = \frac{(U_j + U_i) + \frac{m}{M}U_j}{\left(1 + \frac{m}{M}\right)^2}\frac{d\delta m_j}{dt} + \frac{1}{\left(1 + \frac{m}{M}\right)^3}\frac{U_i^2}{R}\frac{dm}{db},$$ (A12)

$$[F_z]_2 = (U_j + U_i)\frac{d\delta m_j}{dt},$$ (A13)

$$[F_z]_3 = \frac{(U_j + U_i) + \frac{m}{M}(U_j - U_m)}{\left(1 + \frac{m}{M}\right)^2}\frac{d\delta m_j}{dt} + \frac{\left(1 + \frac{U_m}{U_i}\right)\left(1 - \frac{m}{M}\frac{U_m}{U_i}\right)}{\left(1 + \frac{m}{M}\right)^3}\frac{U_i^2}{R}\frac{dm}{db}.$$ (A14)

To sum up, Eqs. (A12)–(A14) represent the impact force of the cases of on cavity and inside cavity, jet cavity and inside balloon, and on balloon and inside bowl, respectively.

---

[1] V. Karman, The impact on seaplane floats during landing, Tech. Rep. 321 (National Advisory Committee for Aeronautics, Washington, DC, 1929).

[2] C. Seddon and M. Moatamedi, Review of water entry with applications to aerospace structures, Intl. J. Impact Eng. **32**, 1045 (2006).

[3] O. M. Faltinsen, M. Landrini, and M. Greco, Slamming in marine applications, J. Eng. Math. **48**, 187 (2004).

[4] F. Huera-Huarte, D. Jeon, and M. Gharib, Experimental investigation of water slamming loads on panels, Ocean Eng. **38**, 1347 (2011).

[5] C. Clanet, F. Hersen, and L. Bocquet, Secrets of successful stone-skipping, Nature (London) **427**, 29 (2004).

[6] J. Glasheen and T. McMahon, A hydrodynamic model of locomotion in the basilisk lizard, Nature (London) **380**, 340 (1996).

[7] Y. Jiang, S. Shao, and J. Hong, Experimental investigation of ventilated supercavitation with gas jet cavitator, Phys. Fluids **30**, 012103 (2018).

[8] A. M. Worthington and R. S. Cole, IV. Impact with a liquid surface studied by the aid of instantaneous photography. paper II, Philos. Trans. Royal Soc. London. Series A, Containing Papers of a Mathematical or Physical Character **194**, 175 (1900).

[9] R. Bisplinghoff and C. Doherty, Some studies of the impact of Vee wedges on a water surface, J. Franklin Inst. **253**, 547 (1952).

[10] R. Cointe, Two-dimensional water-solid impact, J. Offshore Mech. Arct. Eng. **111**, 109 (1989).

[11] R. Zhao and O. Faltinsen, Water entry of two-dimensional bodies, J. Fluid Mech. **246**, 593 (1993).

[12] J. O. Marston, T. T. Truscott, N. B. Speirs, M. M. Mansoor, and S. T. Thoroddsen, Crown sealing and buckling instability during water entry of spheres, J. Fluid Mech. **794**, 506 (2016).

[13] S. Thoroddsen, T. Etoh, K. Takehara, and Y. Takano, Impact jetting by a solid sphere, J. Fluid Mech. **499**, 139 (2004).

[14] A. Korobkin and V. Pukhnachov, Initial stage of water impact, Annu. Rev. Fluid Mech. **20**, 159 (1988).

[15] T. T. Truscott, B. P. Epps, and J. Belden, Water entry of projectiles, Annu. Rev. Fluid Mech. **46**, 355 (2014).

[16] T. Miloh, On the initial-stage slamming of a rigid sphere in a vertical water entry, Appl. Ocean Res. **13**, 43 (1991).

[17] M. Moghisi and P. Squire, An experimental investigation of the initial force of impact on a sphere striking a liquid surface, J. Fluid Mech. **108**, 133 (1981).

[18] J. Glasheen and T. McMahon, Vertical water entry of disks at low Froude numbers, Phys. Fluids **8**, 2078 (1996).

[19] T. T. Truscott, B. P. Epps, and A. H. Techet, Unsteady forces on spheres during free-surface water entry, J. Fluid Mech. **704**, 173 (2012).

[20] J. M. Aristoff and J. W. Bush, Water entry of small hydrophobic spheres, J. Fluid Mech. **619**, 45 (2009).

[21] K. G. Bodily, S. J. Carlson, and T. T. Truscott, The water entry of slender axisymmetric bodies, Phys. Fluids **26**, 072108 (2014).

[22] R. C. Hurd, J. Belden, M. A. Jandron, D. T. Fanning, A. F. Bower, and T. T. Truscott, Water entry of deformable spheres, J. Fluid Mech. **824**, 912 (2017).

[23] D. A. Watson, J. M. Bom, M. P. Weinberg, C. J. Souchik, and A. K. Dickerson, Water entry dynamics of spheres with heterogeneous wetting properties, Phys. Rev. Fluids **6**, 044003 (2021).

[24] I. U. Vakarelski, J. O. Marston, D. Y. C. Chan, and S. T. Thoroddsen, Drag Reduction by Leidenfrost Vapor Layers, Phys. Rev. Lett. **106**, 214501 (2011).

[25] M. Elhimer, N. Jacques, A. E. M. Alaoui, and C. Gabillet, The influence of aeration and compressibility on slamming loads during cone water entry, J. Fluids Struct. **70**, 24 (2017).

[26] N. B. Speirs, J. Belden, Z. Pan, S. Holekamp, G. Badlissi, M. Jones, and T. T. Truscott, The water entry of a sphere in a jet, J. Fluid Mech. **863**, 956 (2019).

[27] R. Rabbi, N. B. Speirs, A. Kiyama, J. Belden, and T. T. Truscott, Impact force reduction by consecutive water entry of spheres, J. Fluid Mech. **915**, A55 (2021).

[28] Y. Jiang, Y. Li, J. Guo, L. Yang, and H. Wang, Numerical simulations of series and parallel water entry of supersonic projectiles in compressible flow, Ocean Eng. **235**, 109155 (2021).

[29] S. L. Ceccio, Friction drag reduction of external flows with bubble and gas injection, Annu. Rev. Fluid Mech. **42**, 183 (2010).

[30] H. Y. Hwang and G. A. Irons, A water model study of impinging gas jets on liquid surfaces, Metall Mater Trans B **43**, 302 (2012).

[31] T. Kumagai and M. Iguchi, Instability phenomena at bath surface induced by top lance gas injection, ISIJ Intl. **41**, S52 (2001).

[32] J.-M. Vanden-Broeck, Deformation of a liquid surface by an impinging gas jet, SIAM J. Appl. Math. **41**, 306 (1981).

[33] Y. Jiang, S.-W. Jeong, B.-K. Ahn, H.-T. Kim, and Y.-R. Jung, Experimental investigation of drag characteristics of ventilated supercavitating vehicles with different body shapes, Phys. Fluids **31**, 052106 (2019).

[34] H. W. Coleman and W. G. Steele, *Experimentation, Validation, and Uncertainty Analysis for Engineers* (John Wiley & Sons, 2018).

[35] See Supplemental Material at http://link.aps.org/supplemental/10.1103/PhysRevFluids.8.064005 for the water entry without and with a gas jet (movies S1 and S2) and the formation of different cavity regimes and impact modes (movies S3–S8) under different modified Froude numbers.

[36] T. Grumstrup, J. B. Keller, and A. Belmonte, Cavity Ripples Observed During the Impact of solid Objects into Liquids, Phys. Rev. Lett. **99**, 114502 (2007).

[37] R. B. Banks and D. Chandrasekhara, Experimental investigation of the penetration of a high-velocity gas jet through a liquid surface, J. Fluid Mech. **15**, 13 (1963).

[38] C. Clanet and J. C. Lasheras, Depth of penetration of bubbles entrained by a plunging water jet, Phys. Fluids **9**, 1864 (1997).

[39] H. N. Oguz, A. Prosperetti, and A. R. Kolaini, Air entrapment by a falling water mass, J. Fluid Mech. **294**, 181 (1995).

[40] F. R. Cheslak, J. A. Nicholls, and M. Sichel, Cavities formed on liquid surfaces by impinging gaseous jets, J. Fluid Mech. **36**, 55 (1969).

[41] V. Duclaux, F. Caillé, C. Duez, C. Ybert, L. Bocquet, and C. Clanet, Dynamics of transient cavities, J. Fluid Mech. **591**, 1 (2007).

[42] D. R. Miller and E. W. Comings, Static pressure distribution in the free turbulent jet, J. Fluid Mech. **3**, 1 (1957).

[43] M. Lee, R. Longoria, and D. Wilson, Cavity dynamics in high-speed water entry, Phys. Fluids **9**, 540 (1997).

[44] M.-C. Lin and L.-D. Shieh, Simultaneous measurements of water impact on a two-dimensional body, Fluid Dyn. Res. **19**, 125 (1997).

[45] M. Mordasov and A. Savencov, Analysis of the force action of a gas jet on the surface of a liquid, Tech. Phys. **57**, 350 (2012).

[46] M. Shiffman and D. C. Spencer, The force of impact on a sphere striking a water surface, Tech. Rep. AMG-NYU-133 (Courant Institute of Mathematical Sciences, New York University, 1945).

[47] A. May, Water entry and the cavity-running behavior of missiles, Tech. Rep. 72-2 (Navsea Hydroballistics Advisory Committee, Silver Spring, MD, 1975).

[48] W. Thielicke and R. Sonntag, Particle image velocimetry for MATLAB: Accuracy and enhanced algorithms in PIVLAB, J. Open Res. Softw. **9**, 12 (2021).

[49] A. May and J. C. Woodhull, The virtual mass of a sphere entering water vertically, J. Appl. Phys. **21**, 1285 (1950).